The First Extracellular Loop Domain Is a Major Determinant of Charge Selectivity in Connexin46 Channels

E. Brady Trexler, Feliksas F. Bukauskas, Jack Kronengold, Thaddeus A. Bargiello, and Vytas K. Verselis

Department of Neuroscience, Albert Einstein College of Medicine, Bronx, New York 10461 USA

ABSTRACT   Intercellular channels formed of members of the gene family of connexins (Cxs) vary from being substantially cation selective to being anion selective. We took advantage of the ability of Cx46 to function as an unapposed hemichannel to examine the basis of Cx charge selectivity. Previously we showed Cx46 hemichannels to be large pores that predominantly conduct cations and inwardly rectify in symmetric salts, properties suggesting selectivity is influenced by fixed negative charges located toward the extracellular end of the pore. Here we demonstrate that high ionic strength solutions applied to the extracellular, but not the intracellular, side of Cx46 hemichannels substantially reduce the ratio of cation to anion permeability. Substitution of the first extracellular loop (E1) domain of Cx32, an anion-preferring Cx, reduces conductance, converts Cx46 from cation to anion preferring, and changes the *I-V* relation form inwardly to outwardly rectifying. These data suggest that fixed negative charges influencing selectivity in Cx46 are located in E1 and are substantially reduced and/or are replaced with positive charges from the Cx32 E1 sequence. Extending studies to Cx46 cell-cell channels, we show that they maintain a strong preference for cations, have a conductance nearly that expected by the series addition of hemichannels, but lack rectification in symmetric salts. These properties are consistent with preservation of the fixed charge region in E1 of hemichannels, which upon docking, become symmetrically placed near the center of the cell-cell channel pore. Furthermore, heterotypic cell-cell channels formed by pairing Cx46 with Cx32 or Cx43 rectify in symmetric salts in accordance with the differences in the charges we ascribed to E1. These data are consistent with charged residues in E1 facing the channel lumen and playing an important role in determining Cx channel conductance and selectivity.

INTRODUCTION

Connexins (Cxs) comprise a large multigene family that encodes the protein subunits that form gap junction (GJ) channels. Membranes containing GJ channels are characterized by high electrical conductivity and permeability to large molecules. A diameter of 1–2 nm has been inferred for GJ channels from demonstration of permeability to a variety of fluorescent dyes and biologically active molecules including cyclic nucleotides, amino acids, second messengers, and small peptides (Bennett et al., 1978; Bevans et al., 1998; Kohen et al., 1979; Lawrence et al., 1978; Pitts and Simms, 1977; Saez et al., 1989; Schwarzmann et al., 1981; Sheridan et al., 1979; Subak-Sharpe et al., 1969; Vaney et al., 1998) The diverse nature of these permeants and the presence of GJs in excitable and nonexcitable tissues suggest that these channels serve a wide range of physiological roles by mediating cell-cell communication through electrical transmission as well as through chemical diffusion of small molecules. This inference is now supported by studies of targeted gene disruptions in mice and a growing list of human genetic disorders linked to GJ channel dysfunction (reviewed in Lo, 1999; White and Paul, 1999; Willecke et al., 1999).

To date there are 14 connexin genes identified in rodents, with tissue- and cell-specific, but overlapping patterns of expression (reviewed in Bruzzone et al., 1996; Beyer and Willecke, 2000). Differences in permeability may be one factor in the evolution of connexin diversity, and the expression of certain connexins may reflect a requirement for intercellular transmission or restriction of specific signaling molecules. Early tracer flux studies concluded that there were fixed charges in some GJ channel pores because permeabilities of anionic dyes were depressed more than that predicted based on molecular size and weight (Brink and Dewey, 1980; Flagg-Newton et al., 1979). More recently, exogenous expression of connexins in isolation has shown permeability to vary from cation selective to passing cations and anions more or less equally, or even displaying anion selectivity (Beblo and Veenstra, 1997; Cao et al., 1998; Elfgang et al., 1995; Mills and Massey, 1995; Oh et al., 1997; Veenstra et al., 1994a,b; Wang and Veenstra, 1997; Verselis and Veenstra, 2000). Thus, differences in charge may be one of the criteria by which biological signals are selected for transmission through gap junctions. Synchronized Ca^{2+} oscillations and propagation of Ca^{2+} waves in a number of tissues including glia, epithelia, liver, pancreas, muscle, and bone are mediated, in part, by transmission of intracellular signals through GJs (Boitano et al., 1992; D'Andrea and Vittur, 1996; Finkbeiner, 1992; Young et al., 1996). In astrocytes, there is support for passive diffusion of inositol 1,4,5-trisphosphate (IP_3), rather than Ca^{2+}, as the mechanism by which GJ-mediated Ca^{2+} waves propagate (Sneyd et al., 1998). Decreased intercellular diffusion of IP_3 in hepatocytes of Cx32-deficient mice is

believed to underlie the reduced ability of these cells to mobilize glucose from glycogen stores upon sympathetic nerve stimulation (Nelles et al., 1996; Niessen and Willecke, 2000). Furthermore, there is evidence that in Cx32-deficient hepatocyte junctions, the remaining connexin, Cx26, forms channels that are less permeable to IP$_3$ than Cx32 (Niessen et al., 2000). These data are consistent with the demonstrated ionic selectivities of Cx32 and Cx26 channels (Oh et al., 1997; Cao et al., 1998; Suchyna et al., 1999).

The molecular basis of GJ selectivity is unknown. In this study we sought to identify domain(s) that influence the ability of connexin channels to discriminate among charged inorganic ions. To do so, we used Cx46, which can function as a hemichannel when expressed in single *Xenopus* oocytes (Ebihara and Steiner, 1993; Paul et al., 1991; Trexler et al., 1996). Unlike cell-cell channels, hemichannels are accessible to direct patch recording in excised configurations and thus are amenable to studies of ionic selectivity with conventional techniques. In a previous study, we showed that Cx46 hemichannels have a large conductance and allow passage of large molecules such as tetraethylammonium. In addition, Cx46 hemichannels show a strong preference for cations and display strong inward rectification in symmetric salts (Trexler et al., 1996). This combination of properties suggests that selectivity is strongly influenced by fixed negative charges located toward the extracellular end of the Cx46 hemichannel pore. Here we evaluated the effects of ionic strength on the ratio of cation to anion permeability determined from reversal potentials by the constant field theory of Goldman-Hodgkin-Katz (GHK; see Eisenman and Horn, 1983) and found changes in selectivity consistent with such a location for fixed charges. Furthermore, through domain swapping with Cx32, a connexin that makes channels that prefer anions, we identified the first extracellular loop (E1) as the domain likely to contain these charges. Substitution of Cx32 E1 sequence alone into Cx46 was sufficient to alter charge selectivity from cation to anion preferring and to change hemichannel current rectification from inward to outward. Extension of studies to cell-cell channels showed qualitative agreement with unapposed hemichannels indicating that pore structure is largely conserved in these two configurations of connexin channel. These data are consistent with E1 contributing to the pore of connexin channels.

METHODS

Expression of Cx46 and mutants in *Xenopus* oocytes

mRNA was prepared from appropriately linearized plasmid DNA with the mMessage mMachine T7 RNA kit from Ambion (Austin, TX), according to the manufacturer's protocol. The mRNA was purified using QIAquick PCR purification columns from Qiagen (Valencia, CA). mRNA bound to the column was eluted with 30–40 μl of an aqueous solution of DNA antisense to the endogenous XenCx38 (8 pmol/ml). We used the phospho-

rothioate antisense oligo 5′-GCT TTA GTA ATT CCC ATC CTG CCA TGT TTC-3′, which is complementary to XenCx38 commencing at NT-5 with respect to the ATG initiation codon. Preparation of *Xenopus* oocytes has been described previously (Rubin et al., 1992a,b). Each oocyte was injected with 50–100 nl of the mRNA/antisense solution. Injected oocytes were kept at 18°C in a standard solution containing (in mM) 88 NaCl, 1 KCl, 2 MgCl$_2$, 1.8 CaCl$_2$, 5 glucose, 5 HEPES, and 5 pyruvate, pH 7.6.

Construction of chimeras composed of Cx46 and Cx32

We constructed 14 chimerical connexins containing various domains of Cx46 and Cx32 by the procedure described by Rubin et al. (1992a) or, when possible, by using restriction enzyme sites that are conserved among the two connexins and the chimerical constructs. The domains of the two connexins, based on the alignment published in Bennett et al. (1991), are delimited as follows. Cx46 is divided into NT (Met1-Lys23), TM1 (Val24-Ala41), E1 (Glu42-Arg76), TM2 (Phe77-Gly94), CL (His95-Val156), TM3 (Phe157-Phe175), E2 (Leu175-Thr207), TM4 (Ile208-Leu226), and CT (Glu227-Ile416). Cx32 is divided into NT (Met1-Arg22), TM1 (Val23-Ala40), E1 (Glu41-Arg75), TM2 (Leu76-Met93), CL (His94-Tyr135), TM3 (Val136-Leu155), E2 (Leu156-Lys187), TM4 (Thr188-Ala207), and CT (Glu208-Cys283). In our notation, a chimera designated as Cx46*Cx32E1 has the sequence of the E1 domain of Cx46 replaced with that of Cx32. In Cx46*32NTM2, all Cx46 sequences from NT through M2 have been replaced by Cx32. Furthermore, in Cx46*32NTM1+M2, in addition to the NT through M1 domains, M2 has also been replaced by Cx32, but E1 remains from Cx46. The list of chimeras and their abilities to form hemichannels are shown in Table 1. All constructs were sequenced over the restriction sites used for cloning, even those in which PCR was not involved.

Construction of vectors and transfection of mammalian cells

The *Eco*R1/*Hind*III fragment from the Cx46-pGem construct containing the entire rat Cx46 coding sequence was blunt-end ligated into pCl-Neo (Promega, Madison, WI) at the *Eco*R1 site for transfection of HeLa cells. Coding sequences from Cx32-pGem and Cx43-pSP72 constructs were subcloned into pCI-Neo using *Eco*RI only. Communication deficient HeLa cells (ATTC number CCL-131) were transfected with these constructs

TABLE 1 Hemichannel function of chimeras formed of Cx46 and Cx32 expressed in *Xenopus* oocytes

Chimera	Hemichannels
Cx46*32NTM2	No
Cx32*46NTM2	No
Cx46*32NTM1	*
Cx32*46NTM1	Yes
Cx46*32E1M2	Yes
Cx32*46E1M2	No
Cx46*32NTE1	No
Cx32*46NTE1	No
Cx46*32M2	*
Cx32*46M2	No
Cx46*32E1	Yes
Cx32*46E1	No
Cx46*32NTM1+M2	No
Cx32*46NTM1+M2	No

*Occasionally observed macroscopic currents, but expression was low and inconsistent among batches of *Xenopus* oocytes.

using lipofectin (GIBCO BRL, Gaithersburg, MD) according to the manufacturer's protocol. Transfected cells were selected and maintained with 300 mg/ml (active) G418 (GIBCO BRL). Positive clones were screened by dual whole-cell patch recordings.

Bath and recording solutions

In macroscopic recordings of Cx46 hemichannel currents, *Xenopus* oocytes were bathed in a modified ND96 solution containing (in mM) 88 NaCl, 1 KCl, 2 MgCl$_2$, 1.8 CaCl$_2$, 5 glucose, and 5 HEPES, pH 7.6. Both current-passing and voltage-recording pipettes contained 2M KCl. For patch clamp recordings of Cx46 hemichannel currents, *Xenopus* oocytes were manually devitellinized in a hypertonic solution consisting of (in mM) 220 Na aspartate, 10 KCl, 2 MgCl$_2$, and 10 HEPES and then placed in the ND96 solution with no added Ca^{2+}. Patch pipette solutions used for recording Cx46 hemichannels consisted of (in mM) 100 KCl, 1 HEPES, 1 EGTA, and 1 MgCl$_2$, and pH was adjusted to 7.5 with KOH.

In whole-cell patch recordings of transfected mammalian cells, the bath solution was a modified Krebs-Ringer consisting of (in mM) 140 NaCl, 4 KCl, 2 CaCl$_2$, 1 MgCl$_2$, 5 HEPES, 5 glucose, and 2 pyruvate, and pH was adjusted to 7.4 with NaOH. Patch pipette solutions consisted of (in mM) 140 KCl, 1 MgCl$_2$, 5 HEPES, 5 EGTA, and 1.4 CaCl$_2$, and pH was adjusted to 7.2 with KOH.

Dye injection studies

Tracer flux was assessed qualitatively by using Lucifer Yellow (LY) (Sigma, St. Louis, MO) and 4′,6-diamidino-2-phenylindole (DAPI) (Molecular Probes, Eugene, OR). Dyes were prepared as 0.1% solutions in the pipette-filling solution. In each cell pair examined, a whole-cell recording with a dye-filled pipette was established on one cell and a gigaohm seal with pipette solution only on the other cell; the patch on the second cell was not ruptured. This procedure allowed dye spread into the recipient cell without loss caused by dialysis with a patch pipette. Fluorescent images were acquired every 5 s (0.5-s exposures) over a period of 5–10 min. A whole-cell recording was then established in the recipient cell to measure g_j. Fluorescence images were obtained with a MERLIN imaging system (LSR, Cambridge, UK) equipped with an UltraPix FE250 cooled digital camera (12 bit) and a SpectraMASTER high-speed monochromator.

Electrophysiological recording and analysis

Voltage clamp recordings of macroscopic Cx46 hemichannel currents from single *Xenopus* oocytes were obtained with a two-electrode voltage clamp (GeneClamp 500, Axon Instruments, Foster City, CA). Currents were digitized using pClamp 6.0 software and a Digidata 1200 interface (Axon Instruments).

Cell-cell channel currents were recorded from transfected HeLa cell pairs using the dual whole-cell patch clamp technique (Neyton and Trautmann, 1985) and two EPC-7 patch clamp amplifiers (Instrutech, Port Washington, NY). To evaluate g_j in cell pairs, both cells were maintained at the same holding potential from which voltage steps, ΔV_j, were applied to one cell. Junctional current was measured directly as the change in current in the unstepped cell, ΔI. g_j is thus given by $\Delta I/\Delta V_j$.

For reversal potential measurements in cell pairs, one patch pipette solution consisted of (in mM) 1 EGTA, 1 HEPES, and 150 KCl. The other patch pipette was filled with the same solution except that KCl was reduced to 50 mM; PEG-600 was added to osmotically balance and minimize streaming potentials. The bath was connected to a ground chamber containing 150 mM KCl pipette-filling solution via a 3 M KCl agar bridge. Instrumentation offsets were nulled with the tips of the pipettes in a stream of 3 M KCl, rather than in bath solution, to minimize the liquid junction potentials between the differing pipette solutions and the bath solution.

Once the dual whole-cell patch was established and the 50 mM and 150 mM solutions were in contact, if the junction potentials between the pipettes and the bath solution had been nulled, an error would have been introduced equal to the difference between the liquid junction potentials generated at the two pipettes (~3.5 mV in ND96 bath); this difference is reduced to ~0.2 mV by nulling in 3 M KCl. After offset correction in 3M KCl, whole-cell patches were obtained on two separate cells previously detached from the coverslip with a gentle stream of bath solution. The cells were then brought into contact. Before the appearance of coupling, the holding current for each cell (I_1 and I_2) was determined solely by its input conductance and represents the baseline current at which reversal of junctional current I_j must be measured. If the salt composition differs between the cells, the appearance of a selective GJ channel will introduce a battery between the cells even in the absence of an applied V_j. This condition generates equal and opposite current flow in both clamps, offsetting the baseline holding currents ($\Delta I_1 = -\Delta I_2$). We applied voltage ramps from −100 to +100 mV to cell 1 and recorded I_j in cell 2 held at constant voltage. The reversal potential of I_j was measured as the potential at which I_j crosses the value of I_2 in the absence of coupling.

Single Cx46 and chimeric hemichannel currents in *Xenopus* oocytes were recorded using an Axopatch 200B (Axon Instruments) with the headstage in capacitive feedback mode. Devitellinized oocytes were placed in a bath chamber filled with a solution containing (in mM) 100 KCl, 1 MgCl$_2$, and 5 HEPES, pH 7.6. The bath chamber was connected via a 3 M agar bridge to a ground chamber containing 100 mM KCl pipette-filling solution. Patch pipettes were filled with the same 100 mM KCl solution. Excised patches were placed in a stream of 100 mM KCl and instrumentation offsets were manually corrected. The concentration of KCl in the stream was then varied by flowing KCl solutions differing in concentration from 10 mM to 1 M through a 7-to-1 manifold. Reversal potentials (V_{REV}) were determined by fitting an exponential or linear function of voltage to the open state current recorded during voltage ramps from −70 to +70 mV. The V_{REV} for a given solution was the average of 10 consecutive ramp current reversals. All V_{REV}s reported are the mean and SEM of multiple patches. Junction potentials between the streams and the KCl bath were small (maximally ~0.4 mV when streaming 1 M KCl) and were not corrected. Patch clamp data from both hemichannels and cell-cell channels were acquired with AT-MIO-16X D/A boards from National Instruments (Austin, TX) using our own acquisition software.

I-V curves were modeled with an early version of Dr. Chen's code for solving the PNP equations that is available at http://144.74.27.66/pnp.html. We benefited from a graphical interface to the PNP program from Traynelis and Dingledine that is available at the same web site. Briefly, the settings we used for the PNP parameters were as follows: number of mesh points = 100, maximum number of iterations = 20,000, tolerance = 1 × 10^{-10}, pore radius = 5.75 Å, pore length = 50 Å, dielectric of membrane = 4, dielectric of aqueous pore = 80, diffusion coefficient of cation = 1.96 × 10^{-5} cm^2/s (K$^+$), and diffusion coefficient of anion = 2.03 × 10^{-5} cm^2/s (Cl$^-$). We did not use the modified Poisson equation that includes induced charge effects.

RESULTS

Application of PNP theory to model Cx46 hemichannels

Because of the large size of GJ channels, we chose to examine mechanisms of conductance and selectivity using a model based on electrodiffusion. Unlike narrow, highly selective ion channels, ions traversing GJ channels need not move in single file or require dehydration to fit through selectivity filters. There is evidence that small ions, and even larger dye molecules, move through GJs in their hydrated forms (Brink, 1983; Verselis and Brink, 1986).

We chose to use PNP, which has been shown to successfully model the *I-V* relationships of several ion channels in a variety of solutions using relatively simple fixed charge distributions (Chen et al., 1997, 1999; Nonner et al., 1998; Nonner and Eisenberg, 1998; Oh et al., 1999). Our goal was not to derive a unique set of parameters from fits to the data, but to use PNP to examine if a charge profile, representing our expectation that there is a dominant negative charge located toward the extracellular end of the hemichannel, could capture the essential features of conductance and selectivity of open Cx46 hemichannels. The features of the Cx46 hemichannel that we strove to reproduce were high conductance, inward rectification, and cation selectivity. Remarkably, a charge distribution that contained a single fixed negative charge density (4 M = $0.25e$/Å) located toward the extracellular end (Fig. 1 *A*) reproduced the essential features of Cx46 hemichannels under a variety of conditions. Experimentally, we used KCl solutions and in modeling the wild-type hemichannel assigned bulk solution values of the diffusion coefficients for K^+ and Cl^-. A pore length of 50 Å and a radius of 5.8 Å produced *I-V* characteristics in good agreement with those measured experimentally in 100 mM KCl over ± 70 mV (Fig. 1 *B*). The calculated relative permeabilities of K^+ and Cl^- and the shapes of the *I-V* relationships in this model pore were also in agreement with those measured in 500:100 mM KCl gradients (Fig. 2).

High extracellular KCl substantially weakens cation selectivity of Cx46 hemichannels

The influence of fixed charges on permeability in a channel can be examined by screening in solutions of high ionic strength (Green and Andersen, 1991). With negative charges positioned toward the extracellular end of the hemichannel pore, extracellular solutions should have a greater charge screening effect than intracellular solutions of the same composition. Experimentally, this phenomenon can be measured as a difference in current reversal potentials for opposite orientations of the same salt gradient. A dependence of selectivity on the orientation of concentration gradients has been shown previously for the synthetic LS channel (Kienker et al., 1994; Kienker and Lear, 1995; Chen et al., 1997).

Inside-out and outside-out patches containing one or two Cx46 hemichannels were placed in test KCl solutions ranging in concentration from 0.01–1.0 M; the concentration in the patch pipette was constant at 100 mM KCl (Fig. 2). Examples of hemichannel currents in response to voltage ramps are shown for patches placed in 500 mM KCl, which exposed hemichannels to a 500:100 mM gradient. Current flowing through open Cx46 hemichannels reversed at -29 mV with high KCl on the cytoplasmic side (Fig. 2 *A*), and at $+23$ mV with high KCl on the extracellular side (Fig. 2 *B*). Fig. 2 *C* shows mean reversal potential plotted versus
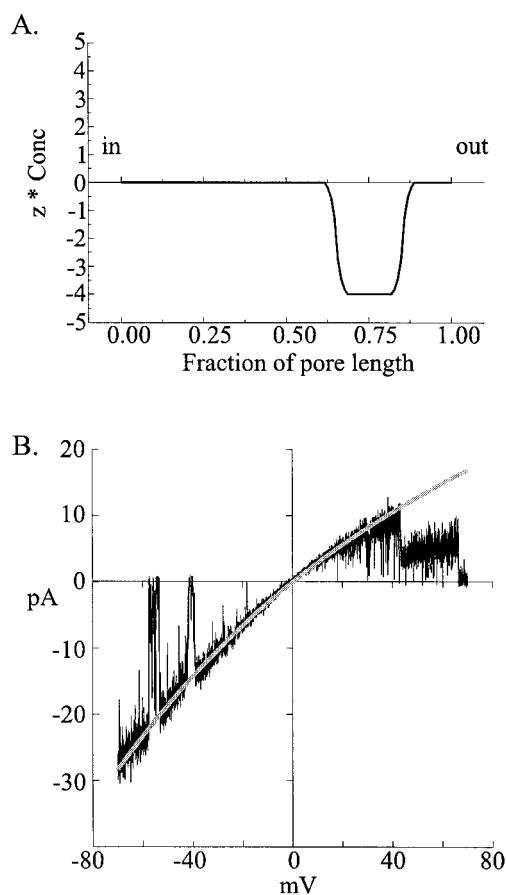

FIGURE 1 The inward rectification of Cx46 hemichannels in symmetric 100 mM KCl can be attributed to fixed negative charges toward the extracellular end of the pore. (*A*) The graph represents a negative charge region (4 M) occupying 20% of the length of the pore that is centered at 75% of the distance toward the extracellular end. (*B*) Recording of a Cx46 hemichannel current in *Xenopus* oocytes obtained with an 8-s voltage ramp from -70 mV to $+70$ mV applied to an inside-out patch containing a single hemichannel. Current was recorded in symmetric 100 mM KCl. From an exponential fit to the open state (not shown), we determined slope conductance to be 300 pS at V = 0 mV, and the open Cx46 hemichannel current varied from -28 pA at -70 mV to 14.4 pA at $+70$ mV. The solid line shows the current obtained with the PNP equations using the charge profile shown in *A* with radius = 5.75 Å and length = 50 Å. Diffusion coefficients were 1.96×10^{-5}/cm^2 s for K^+ and 2.03×10^{-5}/cm^2 s for Cl^-. The PNP-generated current varied from -28 pA at -70 mV to 16.3 pA at $+70$ mV. The hemichannel exhibits two gating behaviors, full closure at negative voltages and partial closure at positive voltages, as demonstrated previously in Trexler et al., 1996. Currents were filtered at 2 kHz and data were acquired at 10 kHz.

test solution concentration. At concentrations exceeding 300 mM, the magnitude of the reversal potential with high KCl on the extracellular side is substantially smaller than that with the same KCl concentration on the inside. The theoretical reversal potentials (solid lines) obtained with PNP theory using the simple charge profile in Fig. 1 *A* agree well with the experimental results. Using the calculated activities of both solutions and the GHK voltage equation,
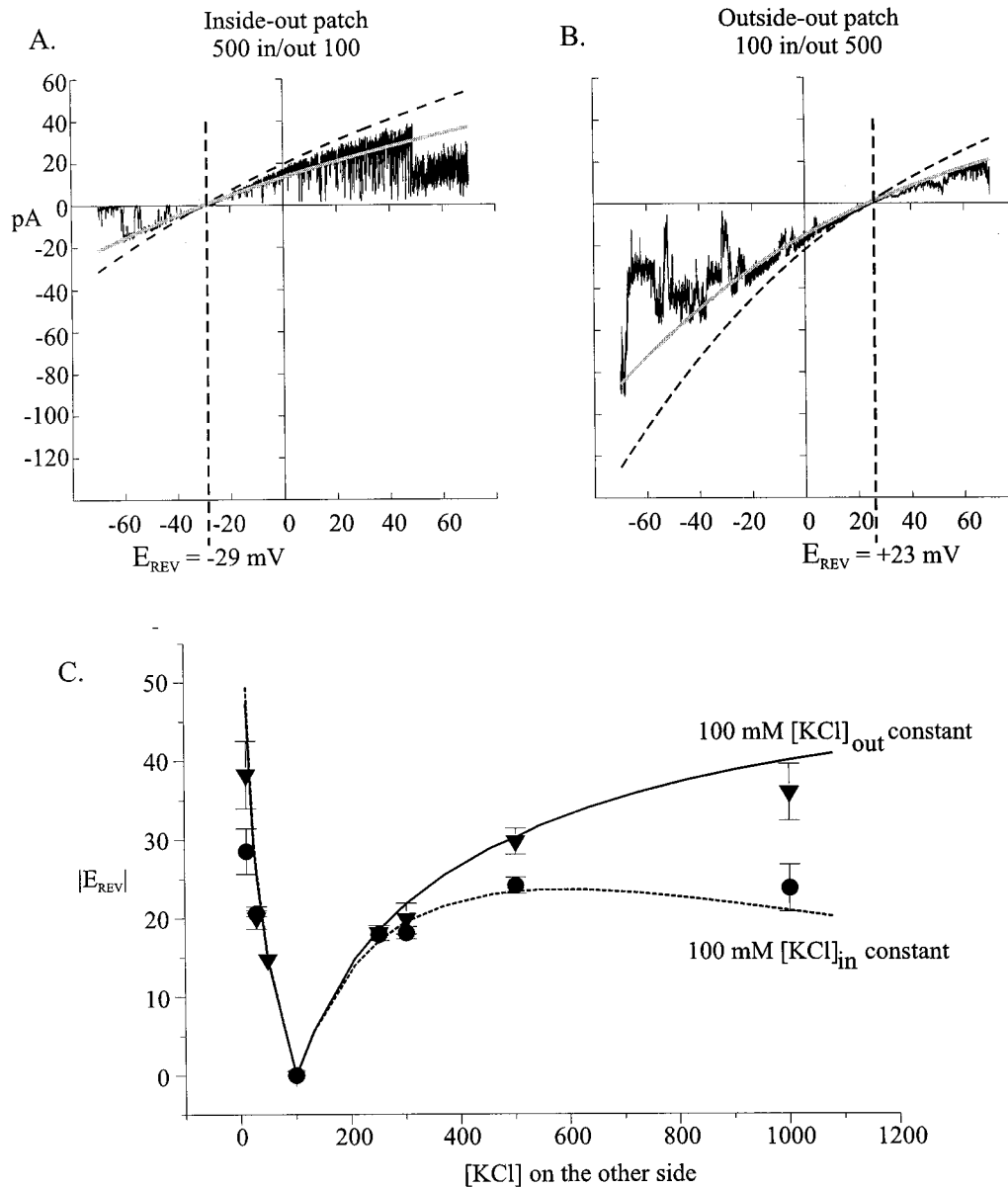
FIGURE 2 The differences in the reversal potentials in oppositely oriented concentration gradients confirm the extracellular placement of the fixed negative charges that govern selectivity. (A) Recording of single Cx46 hemichannel current in a 500:100 KCl gradient with high salt on the cytoplasmic side. The patch was excised in an inside-out configuration. Current reversed at −29 mV in this case. The dashed line is the PNP-generated current using the same parameters as in Fig. 1. The solid line is the PNP-generated current scaled to better fit the data by reducing mobilities of K^+ and Cl^- by 35%. The shapes of the PNP-generated I-V curves, with and without scaling, are in good agreement with the experimental data. (B) Recording of current in a different patch containing two hemichannels placed in a 500:100 KCl gradient with high salt on the extracellular side. The patch was excised in an outside-out configuration. Current reversed at +23 mV in this case. Dashed and solid lines have the same meanings as in A. (C) Plot of absolute value of mean reversal potential as a function of concentration gradient for high salt on the cytoplasmic side obtained from inside out patches (▼) and high salt on the extracellular side obtained from outside-out patches (●). In each case, the pipette solution consisted of 100 mM KCl and the excised patches were perfused with solutions of KCl varying in concentration from 10 mM to 1 M. The dotted and solid lines are the PNP-generated reversal potentials using the charge profile in Fig. 1 A for high salt on the extracellular and cytoplasmic sides, respectively. With [KCl] ≥ 300 mM, reversal potentials decreased markedly with high salt on the extracellular side relative to high salt on the cytoplasmic side, consistent with placement of the negative charges toward the extracellular end of the pore. Currents were filtered at 1 kHz and data were acquired at 10 kHz.

the calculated $P_K:P_{Cl}$ ratio declined from ~13:1 in a 500 mM (in):100 mM (out) gradient to ~6:1 in the same, but oppositely oriented, gradient, 100 mM (in):500 mM (out).

Similar results were obtained with 100:500 mM NaCl gradients (data not shown) indicating that these effects on reversal potential are independent of ion species and likely

to result from charge screening, rather than specific binding of K^+ (Green and Andersen, 1991). The shapes of the single-channel *I-V* relations obtained with PNP in the various salt gradients are in agreement with those observed experimentally (shown only for the 100:500 mM salt gradients, Fig. 2, *A* and *B*). However, the PNP-generated conductances were ~35% higher than those measured and could be corrected by reducing the pore radius or ionic mobilities. These data confirm that negative charges toward the extracellular end of the Cx46 hemichannel pore strongly influence charge selectivity.

Cx46 cell-cell channels: selectivity

An important question is whether selectivity of Cx46 cell-cell channels is the same as that of unapposed Cx46 hemichannels; structural rearrangements associated with hemichannel docking could change the properties of the pore. As a qualitative assessment of charge selectivity of Cx46 cell-cell channels, we transfected HeLa cells with Cx46 and examined cell-to-cell transfer of charged dyes. We used LY, a negatively charged dye with a molecular weight of 443 and DAPI, a positively charged dye with a molecular weight of 280. So that we could examine tracer flux between two cells and assess g_j between them, we used isolated cell pairs only, imaging dye flux and subsequently measuring g_j with the dual whole-cell patch clamp technique in the same cell pair. No spread of LY was detected in Cx46 cell pairs that exhibited strong electrical coupling, i.e., $g_j > 10$ nS ($n = 7$). Conversely, DAPI spread in all Cx46 cell pairs tested that had comparable levels of coupling ($n = 6$). Examples are shown in Fig. 3 *A*. Using the same procedures on HeLa cells transfected with Cx32 and g_j values in the same range, cell pairs expressing Cx32 showed strong LY coupling, in agreement with previously published reports (Cao et al., 1998; Elfgang et al., 1995). Although DAPI is smaller than LY, no DAPI spread was detected between Cx32 cell pairs (Fig. 3 *B*). These data suggest that Cx46 cell-cell channels, like Cx46 hemichannels, prefer cations and that Cx32 cell-cell channels prefer anions. The latter is in agreement with ionic permeability studies of Cx32 (Oh et al., 1997; Suchyna et al., 1999). Both LY and DAPI were permeable to Cx43, indicating poor discrimination based on charge (Fig. 3 *C*).

Given that fluorescent tracers are large molecules that differ in charge, as well as in size and chemical structure, we sought to evaluate the ability of Cx46 cell-cell channels to select between K^+ and Cl^- by measuring current reversal potentials in KCl gradients. Such measurements have been problematic in cell-cell channels because gradients tend to collapse due to mixing of pipette solutions between small, well-coupled cells. In addition, the baseline membrane currents for each cell must be measured in the absence of coupling to determine the level at which the junctional current (I_j) reversal must be measured. Often this baseline

current cannot be evaluated without uncoupling agents. However, no specific uncoupling agents for GJs have been identified and most uncouplers modify nonjunctional membrane currents as well, thereby shifting the baseline current independent of coupling. We resolved these problems by applying a technique whereby individual cells are whole-cell patch clamped and placed into contact to promote de novo coupling (Bukauskas et al., 1995a; also see Methods). In this technique, coupling develops with the appearance of a single channel, followed several minutes later by a second channel and so on. This procedure allows holding membrane currents to be evaluated in each cell in the absence of coupling without pharmacological intervention and, in the same cell pair, allows current reversal to be measured at the level of a single channel. With a single channel connecting two cells, mixing of gradients is negligible.

An example of a recording employing the technique of de novo channel formation is shown in Fig. 4 *A* for HeLa cells transfected with Cx43. Patch pipettes for both cells contained 140 mM KCl. Shown is junctional current I_j recorded in response to small, repetitive transjunctional voltage (V_j) steps applied to the newly formed cell pair. Before the appearance of electrical coupling, the V_j steps elicited no corresponding I_j steps. The appearance of the first channel occurred ~25 min into the recording and I_j increased thereafter for an additional 15 min to reach a near-steady level of ~300 pA, corresponding to ~120 open channels. The boxed region shows the time window between the appearance of the first channel and the appearance of a second channel.

Fig. 4, *B* and *C*, illustrates the use of this technique to measure selectivity of Cx43 and Cx46 cell-cell channels. Patch pipettes, in these cases, differed 150:50 in KCl concentration. Isoosmotic conditions were maintained with PEG-600 added to the low concentration side. Shown in each case are recordings just before and after the appearance of the first channel. A voltage protocol was repeatedly applied to the cell containing 150 mM KCl that consisted of voltage steps followed by a ramp. In the Cx43 cell pair (Fig. 4 *B*), the first appearance of a channel caused no shift in current in the unstepped cell at $V_j = 0$, consistent with a lack of charge selectivity between K^+ and Cl^- ($E_{rev} \approx 0$, shaded bars are when $V_j = 0$). Also consistent with a lack of selectivity is a linear single-channel *I-V* relation in the presence of a KCl gradient. The hydrodynamic radius of PEG-600, estimated to be ~8 Å (Bezrukov and Vodyanoy, 1993; Oh et al., 1997) is larger than that of the Cx43 channel, estimated at ~6.3 Å (Wang and Veenstra, 1997).

In contrast, the appearance of a channel between Cx46-expressing cells (Fig. 4 *C*) shifted current negative in the unstepped cell at $V_j = 0$. The voltage at which I_j crosses the current level before coupling is −18 mV, which gives $P_K:P_{Cl} \approx 7:1$ using the GHK voltage equation. Also, the single-channel current rectified accordingly, with greater current when the high concentration cell (150 mM) was
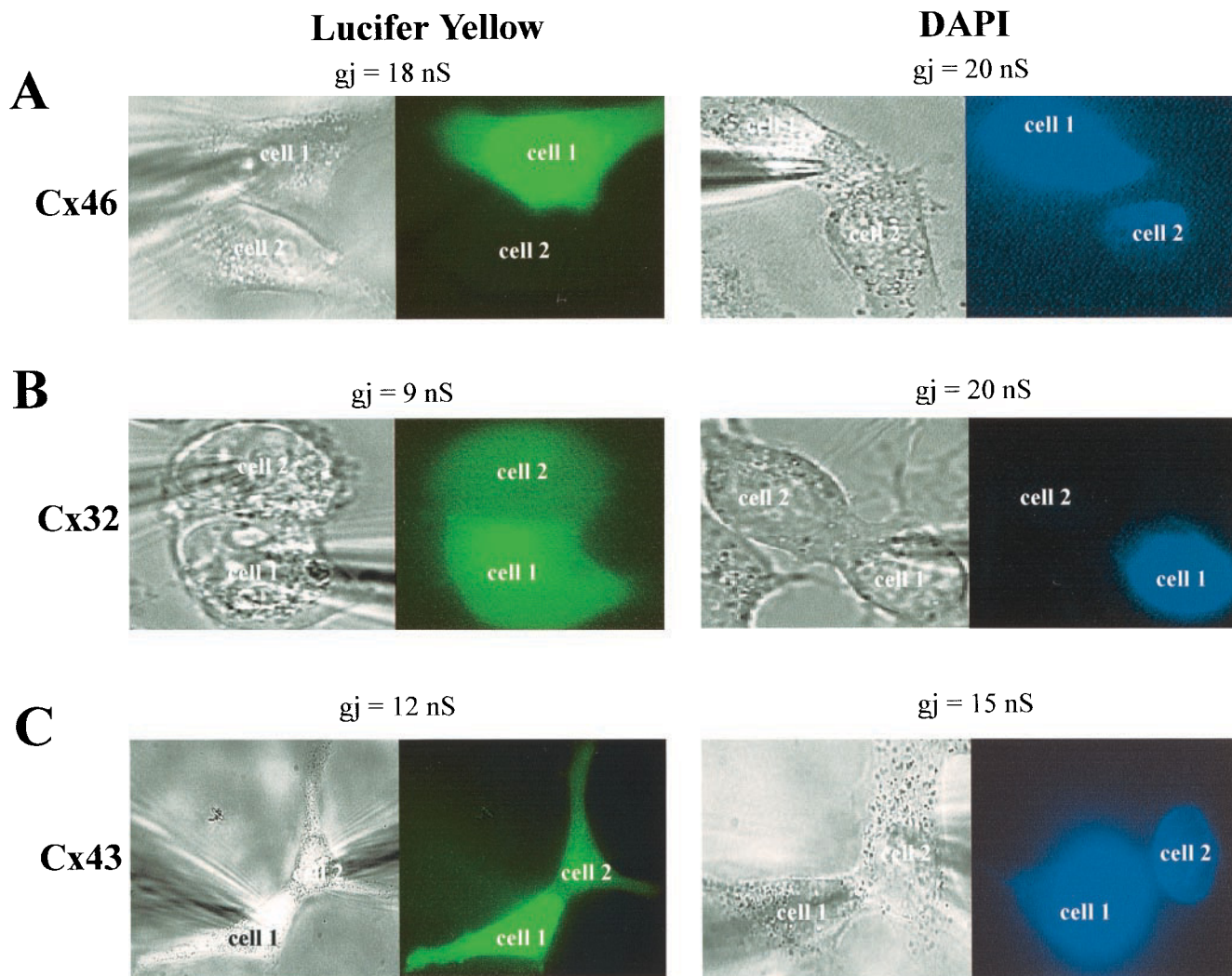
Lucifer Yellow   **DAPI**

gj = 18 nS   gj = 20 nS

A

Cx46

gj = 9 nS   gj = 20 nS

B

Cx32

gj = 12 nS   gj = 15 nS

C

Cx43

FIGURE 3   Connexins have different permeabilities to charged fluorescent tracers. Cell-cell channels between HeLa cell pairs expressing Cx46 (*A*), Cx32 (*B*), or Cx43 (*C*) were assessed for their ability to transfer of LY (molecular weight = 443, $z = -2$) and DAPI (molecular weight = 280, $z = +2$). In each example shown, a whole-cell patch was obtained on cell 1 with a dye-filled pipette. A cell-attached patch was obtained on cell 2 to prevent dialysis of any dye transferred through the junction. Dye transfer was assessed after 5 min, at which time a whole-cell patch was obtained in cell 2 to measure junctional conductance. For Cx46, transfer of DAPI, but not of LY, was detected. For Cx32, transfer of LY, but not of DAPI, was detected. Transfer of both dyes was detected between cells expressing Cx43.

made relatively positive. The mean value of the reversal potential in four experiments was -18.7 ± 2.3 mV. Maintaining the same simple charge profile, radius and length that could account for the conductance and inward rectification of unapposed Cx46 hemichannels (Fig. 1 *A*), we placed two such charge profiles in series, head-to-head (Fig. 5 *A*). With this PNP model, the E_{rev} obtained in a 150:50 gradient was -24 mV, indicating substantial cation selectivity, as in Cx46 hemichannels. Although the E_{rev} obtained with the PNP model was somewhat higher than the mean of -18.7 mV obtained experimentally, these results demonstrate Cx46 cell-cell channels prefer cations over anions much like Cx46 hemichannels.

Cx46 cell-cell channels: conductance and *I-V* relations

I-V relations of single Cx46 cell-cell channels recorded under symmetric conditions are linear (Fig. 5 *B*), in contrast to the inwardly rectifying hemichannels. In addition, the conductance of the cell-cell channel in 140 mM KCl is 140 pS, compared with 300 pS measured as the slope conductance of the hemichannel at $V = 0$ mV in 100 mM KCl. The reduced conductance of nearly half is expected with series addition of hemichannels and is consistent with hemichannels retaining their pore structure when unapposed and when docked in a cell-cell channel configuration. Further-
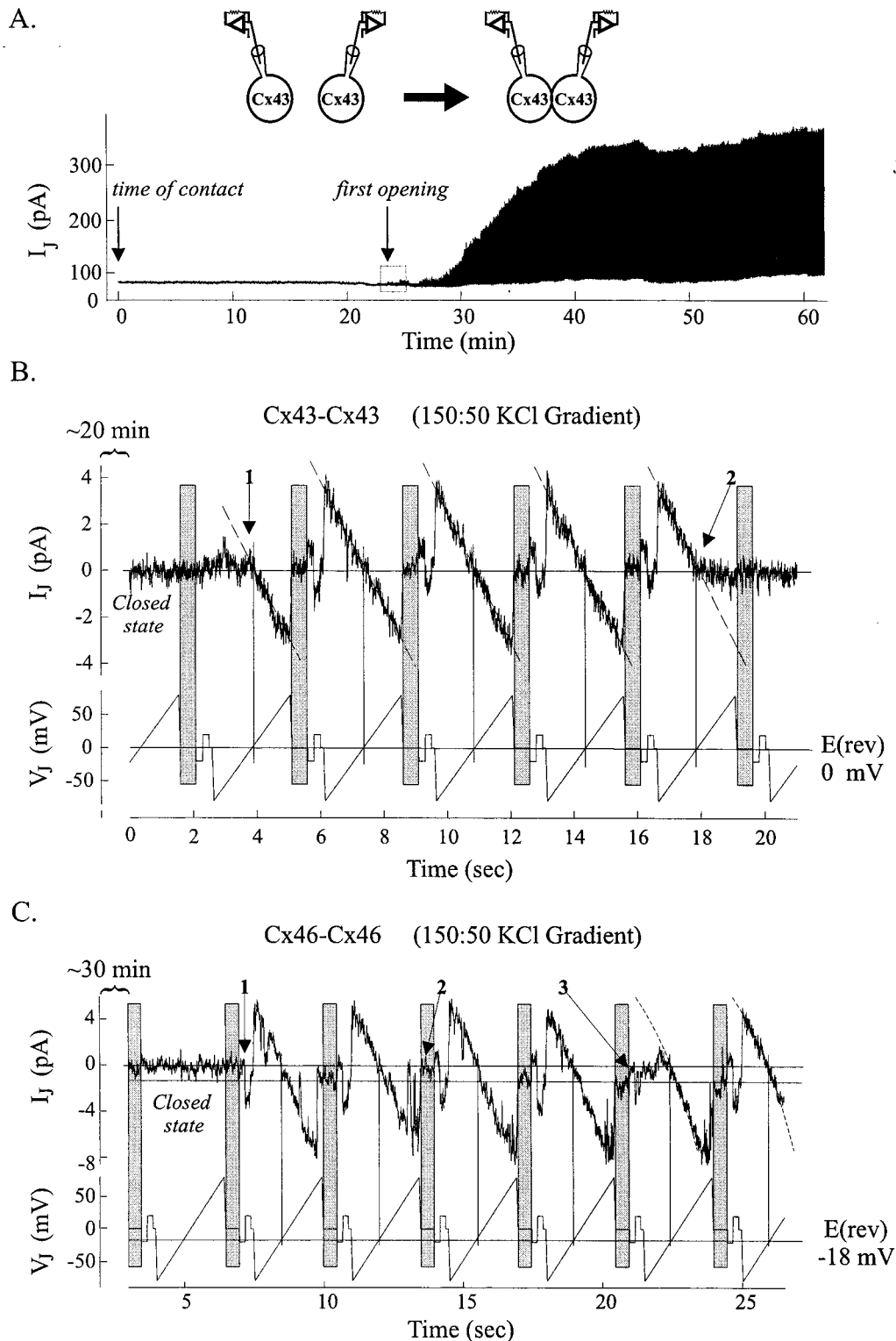
FIGURE 4 Charge selectivity of Cx46 and Cx43 cell-cell channels determined from reversal potentials of single channels in de novo cell pairs. (A) A recording of junctional current between two HeLa cells transfected with Cx43 placed into contact after establishing whole-cell patch clamp recordings in each cell. Small, brief voltage pulses were applied to one cell (not shown) and development of coupling was measured as current deflections in the other cell (I_j). The first appearance of a functional cell-cell channel is indicated (*arrow*), followed by a sigmoidal rise in current due to the formation of additional channels. The boxed region represents the time that only a single cell-cell channel was active. (B) Records of junctional current (I_j) and transjunctional voltage (V_j) obtained from a dual whole-cell recording of a Cx43 HeLa cell pair placed into contact ~20 min before the time series shown. One patch pipette contained 150 mM KCl (cell 1) and the other 50 mM KCl (cell 2). The voltage protocol shown below the current was applied to cell 1 and consisted of
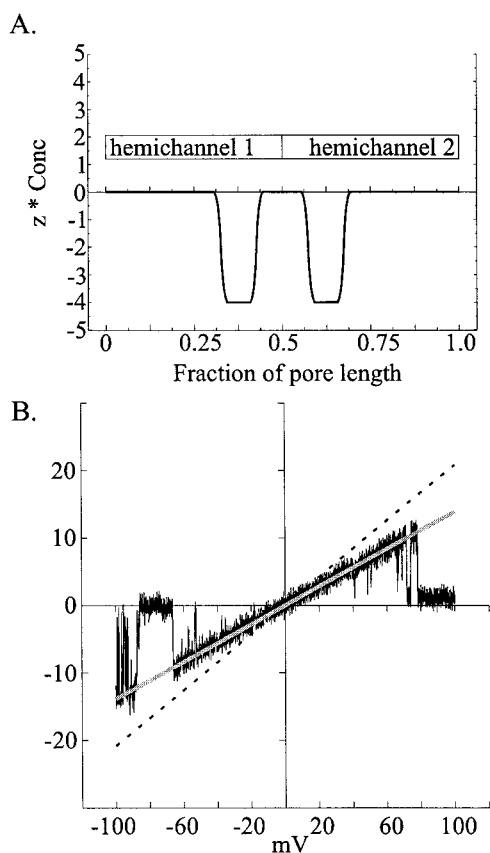
A.

B.

FIGURE 5 The linear *I-V* curve of Cx46 cell-cell channels is consistent with the head-to-head alignment of two hemichannels. (*A*) A charge profile consisting of two Cx46 hemichannels aligned head-to-head. As in Fig. 1 *A*, each hemichannel has a 4 M negative charge region that occupies 20% of its length. (*B*) A record of a single Cx46 hemichannel between two cells in symmetric 140 mM KCl. The voltage in cell 2 was ramped from +100 to −100 mV over a 3-s interval, and the junctional current recorded in cell 1 is shown. In these solutions, Cx46 cell-cell channels have a 140-pS conductance. The dashed line is the current obtained with PNP using the charge profile in *B* and a radius of 5.75 Å, corresponding to a conductance of 200 pS. Decreasing the radius to 4.75 Å or reducing ionic mobilities by 30% (*solid line*) decreased the conductance to 140 pS, in agreement with the data. In both cases, the current is linear, attributable to the symmetry of the cell-cell channel charge profile. Currents were filtered at 1 kHz and data were acquired at 5 kHz.

more, the linearity of the *I-V* relation over ±100 mV is predicted by PNP with maintenance of the simple charge profile we ascribed to unapposed hemichannels; linearity results from an imposition of symmetry of the fixed charge

profile and a change in the relative position of fixed charge toward the center of the channel along its axis. Quantitatively, the 200-pS conductance obtained with the PNP model differs from the measured 140-pS conductance. Thus some changes in the position and/or magnitude of the effective charge or ionic mobilities or channel length or radius may occur as a result of hemichannel docking.

Chimeras composed of Cx46 and Cx32 identify E1 as important for Cx channel selectivity

Considering that Cx32 is anion preferring, as supported by dye diffusion, reversal potential, and ion conduction studies (Fig. 3; Cao et al., 1998; Oh et al., 1997; Suchyna et al., 1999), we constructed chimeras in which segments of Cx46 sequence were replaced with those of Cx32 to identify domains that contribute to differences in charge selectivity among connexins. Each chimera was tested for hemichannel activity whose properties could be examined more easily in excised patches. In total we constructed 14 chimeras (Table 1). Three chimeras, when injected into single *Xenopus* oocytes, consistently produced large, slowly activating membrane currents that are indicative of functional hemichannels. These were Cx32*46NTM1, in which the N-terminus through TM1 of Cx32 was replaced with Cx46 sequence, Cx46*32E1M2, in which E1 through TM2 of Cx46 was replaced with Cx32 sequence, and Cx46*32E1, in which only E1 of Cx46 was replaced with Cx32 sequence. All three chimeric hemichannels have markedly reduced unitary conductances approximately fivefold smaller than wild-type Cx46 hemichannels. The slope conductances of single Cx32*46NTM1, Cx46*32E1M2, and Cx46*32E1 hemichannels at $V_m = 0$ mV are 60 pS, 60 pS, and 55 pS, respectively (Fig. 6), compared with 300 pS for wild-type Cx46.

In addition to smaller conductances, all three chimeric hemichannels display *I-V* relations that are outwardly rectifying in symmetric 100 mM KCl. Cx46*32E1 is the most strongly rectifying with a nearly threefold larger conductance at +70 mV than at −70 mV (Fig. 6 *C*). Substitution with Cx32 E1 sequence alone appears to be sufficient to cause the conversion from inward to outward rectification.

To determine whether a change to outward rectification in the Cx46*32E1 chimera is accompanied by a change in charge selectivity, we examined current reversal potentials

±20-mV steps (250 ms in duration) followed by a ±70-mV ramp (2.5 s in duration). The opening of the first channel occurred during a voltage ramp (*arrow 1*). Successive ramps show the currents reverse at $V_j = 0$ mV, at the level corresponding to $I_j = 0$ pA before the initial channel opening. Thus, Cx43 cell-cell channels are nonselective. The channel spontaneously closes fully during application of the fifth ramp (*arrow 2*). (*C*) The same experiment was performed using Cx46 transfected HeLa cells. After opening of a single channel (*arrow 1*), junctional currents cross the $I_j = 0$ pA level when $V_j = −18$ mV indicating that Cx46 cell-cell channels select K$^+$ over Cl$^-$ at a 7:1 ratio. The last two ramps clearly show rectification such that more current passes from cell 1 (150 mM KCl) to cell 2 (50 mM KCl), consistent with a cation-selective channel. The current levels at arrows 2 and 3 correspond to $I_j = 0$ pA before channel formation. These represent full closures of the Cx46 intercellular channel, a frequent phenomenon in long recordings of these channels (Verselis et al., unpublished results). Currents were filtered at 1 kHz and data were acquired at 5 kHz.
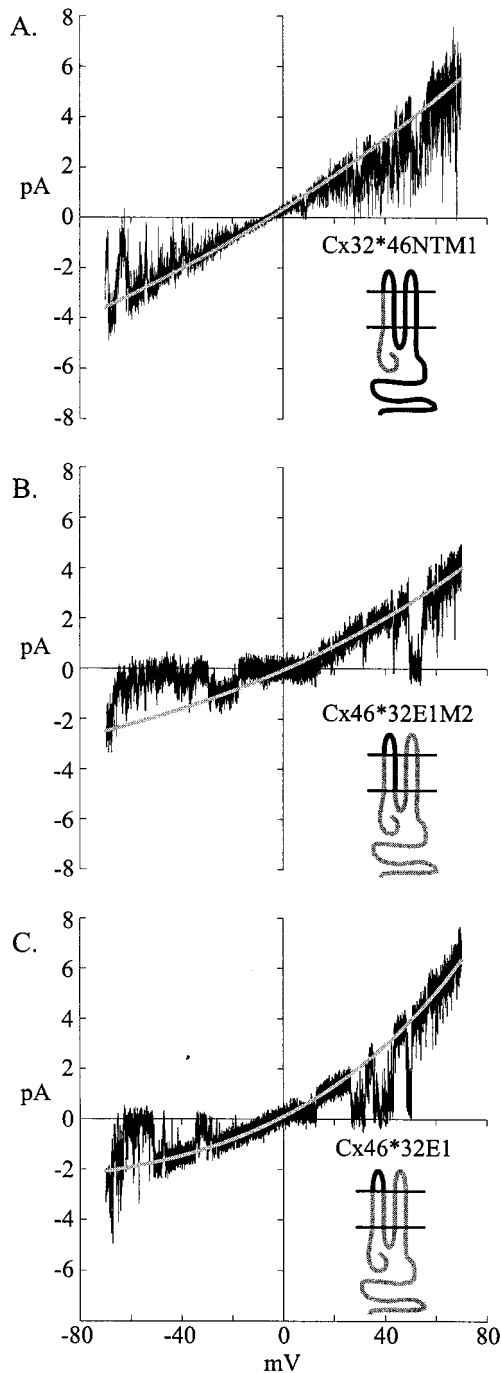
FIGURE 6 The hemichannel conductance and current rectification of chimeric connexins formed of Cx46 and Cx32 differ from wild-type Cx46. Inside-out patches containing a single hemichannel were ramped from -70 to $+70$ mV over an 8-s interval. (*A*, *B*, and *C*) Representative current records that have been leak subtracted. For each, an exponential function was fit to the open-state current (*solid gray line*). From the exponential fit, the slope conductances at $V_m = 0$ mV were (*A*) 60 pS for Cx32*46NTM1, (*B*) 60 pS for Cx46*32E1M2, and (*C*) 55 pS for Cx46*32E1. All three chimeras show outward rectification. The inset in each graph is a schematic representation of the composition of the chimeras; Cx46 sequence is gray and Cx32 sequence is black. The extracellular loops (E1 and E2) are above the two horizontal lines, which represent the limits of the plasma membrane. Currents were filtered at 2 kHz and data were acquired at 10 kHz.

in KCl gradients (Fig. 7). In a 500 mM (in):100 mM (out) KCl gradient, the reversal potential is $+10 \pm 1.5$ mV (SEM, $n = 5$), compared with -30.2 ± 1.2 mV (SEM, $n = 10$) for wild-type Cx46 in the same gradient (Fig. 7 *A*). This change in reversal potential represents a change in selectivity from substantially preferring cations over anions ($P_K/P_{Cl} = 13$) to preferring anions over cations ($P_K/P_{Cl} = 0.5$). Also, as expected for an anion-preferring channel with a higher concentration of permeable anion on the inside, the *I-V* curve in the KCl gradient with high KCl on the inside shifts from outward rectification toward linearity. These data can be explained if substitution of Cx46 E1 sequence with that of Cx32 replaced the negative charge at the extracellular end of the Cx46 hemichannel with positive charge. By reversing the sign and reducing the magnitude of the charge eightfold in our PNP model (Fig. 7 *B*), we could reproduce the charge selectivity of Cx46*32E1 determined from re-
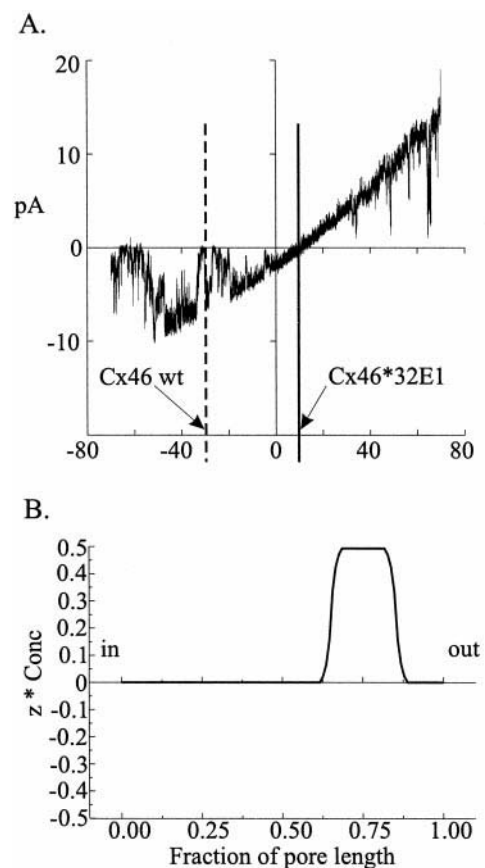

FIGURE 7 E1 is a major determinant of connexin selectivity. (*A*) Replacement of Cx46 E1 with Cx32 sequence changes Cx46 from a cation-selective to an anion-selective hemichannel. In an inside-out patch, the current through a single Cx46*32E1 hemichannel in a 100(out):500(in) KCl gradient reverses at $+10.3$ mV (*solid vertical line*), compared with -30 mV for wild-type Cx46 hemichannels (*dashed vertical line*). Currents were filtered at 1 kHz and data were acquired at 10 kHz. (*B*) Cx46*32E1 selectivity can be modeled by changing the 4 M negative charge in wild-type Cx46 (see Fig. 1 *A*) to 0.5 M positive charge giving a reversal potential of $+10.6$ mV in the same 100(out):500(in) KCl gradient.

versal potentials measured in a 100 mM (out): 500 mM (in) KCl gradient; (E_{rev} = +10.6 mV compared with +10.3 ± 0.8 mV (SEM, n = 3) measured experimentally). However, this magnitude of positive charge in E1 could not produce sufficiently steep rectification of the *I-V* relation and underestimated the reduction in conductance caused by the E1 substitution. An increase in the magnitude or change in the position of the charge could produce steep rectification but rendered the hemichannel too strongly selective for anions. Thus, additional charges and/or geometric considerations are required to model Cx46*32E1 hemichannels. We did not measure selectivity in the other two chimeras because Cx46*32E1M2 rarely opened at voltages more negative than +20 mV and the flickery gating of Cx32*46NTM1 hemichannels in salt gradients precluded accurate reversal potential measurements.

Charges in E1 and *I-V* characteristics of heterotypic cell-cell channels

Attempts to express Cx46*32E1 and Cx32*46E1 in HeLa cells to examine permeability of cell-cell channels formed of these chimeras were not successful. As an alternative means of evaluating the influence of E1 on cell-cell channel permeability, we examined *I-V* relations of single heterotypic channels formed by pairing Cx46 with the other wild-type connexins we examined, Cx43 and Cx32. We maintained a 4 M negative charge in E1 of Cx46 as modeled in Figs. 1 *A* and 5 *A* and a 0.5 M positive charge in E1 of Cx32 hemichannels as modeled for Cx46*32E1 hemichannel selectivity (Fig. 7 *B*). Because of poor charge selectivity of Cx43 channels (Figs. 3 *C* and 4 *B*), E1 of Cx43 was assumed to be uncharged. With these charge profiles, which exclude possible contributions of charges in other domains, heterotypic pairings of these hemichannels will give rise to rectification because of the asymmetries created in the voltage/concentration profiles in the pores.

Placing separate coverslips containing Cx46, Cx43, and Cx32 transfected cells in the same recording chamber, we formed heterotypic channels by the de novo formation method described previously (Fig. 4 *A*). Illustrated in Fig. 8, *A* and *C*, are the charge profiles used to simulate Cx46/Cx32 and Cx46/Cx43 heterotypic channels and corresponding recordings of single channels showing their *I-V* relations; the *I-V* relations generated by PNP are superimposed on the recorded currents (Fig. 8, *B* and *D*). In both cases, the PNP-generated *I-V* relations agree well with the experimental data. Junctional currents are greater when the Cx46 side is made relatively positive, consistent with the greater negativity of E1 in Cx46. Cx46/Cx32 heterotypic channels rectify more than Cx46/Cx43 channels, consistent with the greater predicted asymmetry in charge that would occur by pairing E1 of Cx32 with E1 of Cx46. Cx43, while modeled as an uncharged pore, could be equivalently modeled with fixed positive and negative charges that give rise to nonse-

lectivity and that are distributed such that concentration/voltage profiles produce summed cation and anion fluxes that change linearly with voltage. Although such charges in E1 or in other domains may be present, they are likely to be small and/or offsetting as the essential features of rectification of these heterotypic cell-cell channels can be explained by differences in the charges in E1 we ascribed to the component hemichannels.

DISCUSSION

E1 likely contributes to the lining of the pore in the extracellular gap region of GJ channels

In this study, we sought to determine the mechanism by which connexin channels discriminate among charged ions. Our data indicate that the selectivity of Cx46 hemichannels is strongly influenced by fixed negative charges that are located toward the extracellular end of the hemichannel. Domain substitution with Cx32 sequence identified Cx46 E1 as the domain that contains these charges. Substitution of Cx32 E1 sequence alone converted single Cx46 hemichannel current rectification from inward to outward and changed permeability from cation to anion selective. The simplest interpretation of these results is that the E1 domains of Cx32 and Cx46 contain charge regions of opposite sign. Alternatively, the charge region in E1 of Cx32 may be negative, but substantially smaller in magnitude or absent, thereby allowing a positive charge in another region of the pore to exert a significant influence on conductance and selectivity. This positive charge would also have to be small in magnitude compared with the Cx46 E1 charge and be located in the extracellular half of the pore to account for the outward rectification of the Cx46*32E1 chimera. In either case, a large negative charge region that most strongly influences conductance and selectivity appears to be present in E1 of Cx46. This influence of E1 on selectivity is consistent with its contributing to the lining of the pore.

The negative charge region in E1 effectively influences the selection of cations over anions, but does not influence the selection among monovalent cations (Trexler et al., 1996). This selectivity profile characterizes several types of large cation channels, most notably ACh receptor channels, which permit nearly equal Na$^+$ and K$^+$ fluxes while excluding Cl$^-$ (Adams et al., 1980). In ACh channels, charged residues are responsible for cation selectivity and are arranged in three rings, with the intermediate ring dominant (Imoto et al., 1988; Wilson et al., 2000). In connexin hemichannels, which can be composed of six identical subunits, charges would be contributed by each subunit and would likely constitute a ring much like in ACh channels. The 4M effective negative charge region we used to model Cx46 hemichannels had dimensions of 5.75 Å for the radius and 10 Å for the length, which translates to −2.5 e, or 0.42 e per subunit. These values may be low estimates of the true
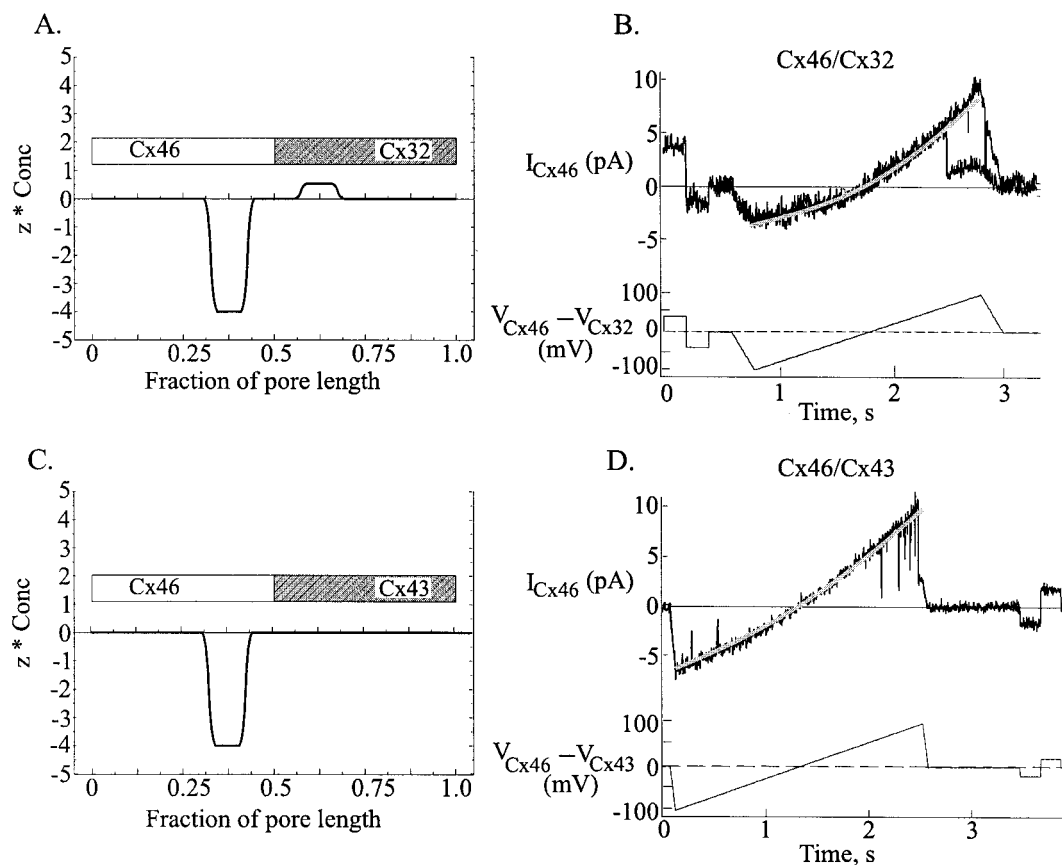
FIGURE 8 Differences in charges in E1 can explain single-channel current rectification in heterotypic pairings of Cx46 with Cx32 or Cx43. (*A*) The charge distribution determined for Cx46*32E1 hemichannels (0.5 M positive charge, Fig. 7 *B*) was used for Cx32 hemichannels in heterotypic pairings with Cx46 (*hatched bar* represents Cx32 side). (*B*) Junctional currents were recorded from the Cx46-expressing cell in response to a voltage protocol applied to the Cx32-expressing cell that consisted of two 200-ms prepulses (± 40 mV) followed by a 2-s ramp from -100 to $+100$ mV. The voltage shown is that of Cx46 relative to Cx32. Two consecutive traces are superimposed in the current record. The current through the fully open state rectifies from -3.6 pA at -100 mV to 9.25 pA at $+100$ mV. Furthermore, the rectification is evident in the asymmetric amplitudes of the junctional current during the prepulses. The solid gray line is the open-state current obtained with PNP, scaled to fit the data by reducing the radius to 4.0 Å or by reducing ionic mobilities by 55%. (*C*) As Cx43 is nonselective, we modeled Cx43 hemichannels as neutral pores (*hatched bar*). (*D*) Heterotypic Cx46/Cx43 cell-cell channels also rectify, passing -6.25 pA at -100 mV and 9.9 pA at $+100$ mV. The solid gray line is the open-state current obtained with PNP scaled to fit the data by reducing the radius to 4.15 Å or by reducing ionic mobilities by 50%. Currents were filtered at 1 kHz and data were acquired at 5 kHz. In both heterotypic channels, cations are the major current carrier due to the dominant negative charge in the Cx46 hemichannels. There is an asymmetric concentration of cations across the pore, providing a greater current source for cation current flowing across the junction from the Cx46 side.

number of charges on the channel wall. A homogeneous distribution of 2.5 *e* throughout the volume of 20% of the pore (see Fig. 1) may correspond to six or more charges on the pore lining. In Cx46 hemichannels, there are five positions in E1 that differ in charge compared with Cx32: 43E/S, 49Q/K, 51D/S, 62E/N, and 68R/H (designated as position Cx46/Cx32). Cx46 is considerably more negative at these positions than Cx32 (-2 vs. $+1$), consistent with the predicted signs of the fixed charges that determine hemichannel rectification and selectivity. However, differences in charge can also arise at positions containing titratable Cys and His residues and from exposed backbone carbonyls or helical dipoles as demonstrated in gramicidin and K^+ channels (Andersen and Koeppe, 1992; Doyle et al., 1998; Roux and Karplus, 1994; Roux and MacKinnon,

1999). Individual amino acid substitutions in E1 will help identify the specific molecular determinants of selectivity. Demonstration of their solvent accessibility would confirm E1 as pore lining.

Recently, a structure of the Cx43 cell-cell channel was determined at ~ 7.5-Å resolution using electron crystallography (Unger et al., 1999). General features of the channel include wide vestibules at the cytoplasmic ends, pronounced narrowing of the pore at the outer membrane borders, and a widening in the region of the extracellular gap. Although details of secondary structure were not revealed, the channel in the extracellular gap gave a double-layered appearance, with the interior layer of protein forming a continuous wall. If this structure is representative of an open channel, our data suggest that E1 forms or contributes

to the inner wall of protein in the extracellular gap. A possible location for the charges in E1 that influence selectivity could be at the pronounced narrowing of the pore at the outer membrane borders, as diagrammed in Fig. 9. Charges at narrowed regions can be more effective at influencing selectivity because of a larger local electrostatic potential in the pore. The narrowness of these regions may also determine the size exclusion limit of the pore. The gross molecular boundaries in the structural studies by Unger et al. (1999) do not reveal positions of side chains, leaving the possibility of having local restrictions in the pore anywhere along the length of the channel.

Hemichannels and cell-cell channels

In experiments that are substantially more difficult than with hemichannels, we also determined that Cx46 cell-cell channels are cation selective, consistent with conservation of the fixed negative charges in both configurations of channel. Whereas this fixed charge is located toward the
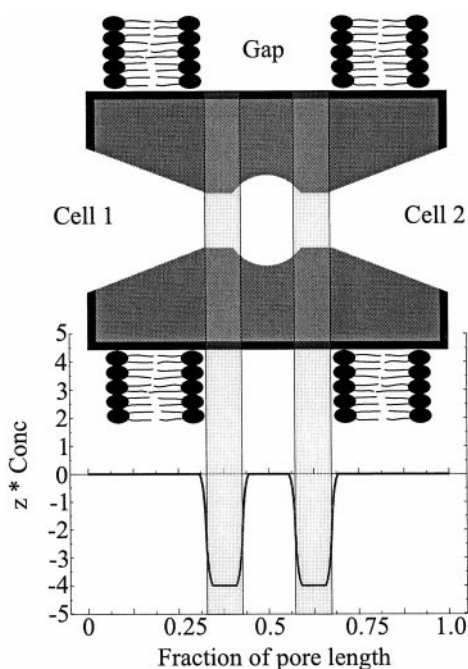

FIGURE 9 Charged regions in E1 may correspond to the constrictions in the pores of intercellular channels. Shown is a contour of the channel pore diagrammed according to the three-dimensional structure determined by Unger et al. (1999), extending slightly outside the confines of the cytoplasmic membrane borders. Excluding contributions of side chains, the pore is widest at the cytoplasmic ends (~40 Å at the membrane border), narrows at the extracellular membrane boundaries to ~15 Å, and widens again in the extracellular gap to ~25 Å. Superimposition of the charged distribution we used in PNP modeling of hemichannels and cell-cell channels shows that the charge regions align close to the constricted regions revealed by the three-dimensional structure. Thus, the constricted regions may serve as charge and size selectivity filters in connexin channels.

extracellular end of the unapposed hemichannel, upon head-to-head docking of hemichannels to form a cell-cell channel, the fixed charge would be located close to the center of the channel. Experimentally, we found the *I-V* curve of Cx46 cell-cell channels to be linear, consistent with that generated using a PNP model with two centrally located fixed charges each representing that ascribed to each unapposed hemichannel. The PNP-generated conductance of the cell-cell channel, based on series alignment of hemichannels, was somewhat larger than what we measured experimentally. One possibility is that the interactions between the extracellular loops of two docked hemichannels slightly alter the charge density relative to that modeled in the unapposed hemichannel. Quantitative differences aside, the essential features of reduced conductance, maintenance of cation selectivity, and linearity of the *I-V* curve is consistent with a series addition of unapposed hemichannels and suggests that no gross changes in hemichannel pore structure occur upon docking to form cell-cell channels. These results indicate that, by and large, permeability studies in hemichannels are likely to be applicable to cell-cell channels as well.

Molecular correlates of fixed charges in connexin pores

Currents flowing through open heterotypic channels formed by pairing Cx46 with either Cx32 or Cx43 rectify in a manner consistent with the net charge in E1 we ascribed from a combination of dye diffusion and ion permeability studies in the corresponding homotypic channels. Likewise, the essence of rectification in heterotypic Cx32/Cx26 channels, originally reported by Bukauskas et al. (1995b), could be explained from the properties of the hemichannels determined from the corresponding homotypic channels (Suchyna et al., 1999). Selectivity characteristics were ascribed to Cx32 and Cx26 hemichannels based on differences in the unitary conductances of corresponding homotypic cell-cell channels in different symmetric salts. In the absence of structural information, the authors placed the charges that give rise to the anion- and cation-preferring selectivities of Cx32 and Cx26, respectively, at the cytoplasmic mouths of the cell-cell channel. Our data suggest that these charges may be located deeper in the pore within the E1 domain of connexins.

In a molecular study of Cx32 and Cx26, charges in NT and at the TM1/E1 border were shown to strongly influence the *I-V* relations of homotypic and heterotypic channels formed of these connexins (Oh et al., 1999). Charges in NT and at the TM1/E1 border were presumed to be located toward the cytoplasmic and extracellular ends of the hemichannel pore, respectively. The *I-V* relation and weak anion selectivity of Cx32 channels was modeled with positive charges at the cytoplasmic ends, attributed to the N-terminal Met residues (M1), superimposed on a smeared

negative charge, perhaps attributed to backbone carbonyls. Cx26 retained the positive charge of M1, but introduced negative charges attributed to the Asp residue at the adjacent position, D2, and internal negative charges at the location of the extracellular loops. The strong rectification of the open heterotypic Cx32/Cx26 channel could be explained by the combination of positive and negative charges at the cytoplasmic ends of Cx32 and Cx26, respectively. In support of this model, substitution of Asp for the Asn at position 2 in Cx32 produced rectification in Cx32/Cx32N2D heterotypic channels similar to that in Cx32/Cx26 heterotypic channels. Ionic selectivity was not assessed in these studies.

In the case of Cx46 hemichannels, the residue in NT at the comparable position, D3, does not appear to have the same influence as in Cx32 or Cx26. This conclusion is based not only on the shapes of the *I-V* relations but on selectivity data as well. Rectification of Cx46 hemichannels is opposite that expected for a significant negative charge at the cytoplasmic end. Also, the greater charge screening effects of extracellular solutions are inconsistent with a dominant cytoplasmic charge. Furthermore, a significant cytoplasmic negative charge, although consistent with strong outward rectification in Cx46*32E1 hemichannels, is inconsistent with its anion selectivity. Finally, although the difference in the permeabilities of Cx32 and Cx26 junctions to LY (Cao et al., 1998) can be explained by an electrostatic effect exerted by the residue at position 2 in NT, the charge at the homologous position in other connexins does not correlate with an ability to pass LY. Both Cx43 and Cx46 contain a negative charge, D3, but permeability of Cx43 to LY is high, comparable to Cx32, whereas LY transfer could not be detected in Cx46-expressing cells.

The differences between the charge profiles of Cx46 compared with Cx32 and Cx26 may be a consequence of structural differences among connexins. Primary sequence comparisons have led to the classification of connexins into two major groups (Bennett et al., 1994). Cx32 and Cx26 belong to group I (β) and Cx46 to group II (α). Mutational studies of voltage gating demonstrated that the charges at the N-terminal end of NT form part of the transjunctional voltage sensor (Verselis et al., 1994). This result suggests that NT is turned back into the membrane, and perhaps into the channel pore, thereby placing the N-terminal end of NT in the field generated by V_j. The effects of charge substitutions in NT of Cx32 on the *I-V* relations of channels formed of Cx32 and Cx26 are consistent with the placement of NT in or near the pore (Oh et al., 1999). Groups I and II connexins differ in the number and position of charges in NT, which could explain the differences in the effects of these charges have on connexin *I-V* relations. The structure of NT of Cx46, and possibly other group II connexins, may differ such that D3 has a weaker effect on permeating ions, perhaps by electrostatic interactions with other residues that differ in group I and group II connexins. This possibility can be addressed by examining the effects of substitutions both in NT and E1 on *I-V* relations of Cx46 and chimeric Cx46 hemichannels.

Chimeras of Cx46 and Cx32: TM1 and channel conductance and selectivity

Structure/function studies aimed at identifying pore-lining domains in connexin channels have been largely based on effects of mutations on single-channel conductance or permeation of uncharged molecules. Several reports have implicated TM1 as a pore-lining domain. In Cx32, a mutation in TM1 of Cx32 associated with Charcot-Marie-Tooth disease, S26L, restricted the size of permeating uncharged molecules from $\sim$7 Å to $\sim$3 Å (Oh et al., 1997). In Cx46 and Cx32*43E1 hemichannels, residues toward the extracellular end of TM1 were reported to be accessible to cysteine-modifying reagents (Zhou et al., 1997). Furthermore, Hu and Dahl (1999) reported Cx32*43E1 hemichannels to have a conductance smaller than Cx46 and that replacement of TM1 of Cx46 into Cx32*43E1 hemichannels increased the conductance similar to that of Cx46. This conductance effect was interpreted as an exchange of permeation pathways formed by TM1. However, the three chimeric hemichannels we examined had conductances fivefold less than Cx46, yet contained TM1 of Cx46 in each case. Also, the charge selectivities of wild-type Cx46 and chimeric Cx46*32E1 hemichannels, assessed from reversal potentials in 500 mM (in):100 mM (out) KCl gradients, markedly differ yet both hemichannels contain TM1 of Cx46. Thus, our data do not support TM1 as the key determinant of single-channel conductance or selectivity in Cx46 hemichannels but do not rule out TM1 as a pore-lining domain.

PNP and insights gained into connexin pore structure

We chose to model connexin permeation with PNP because it is fundamentally a charge-screening model suitable for examining how positions and magnitudes of fixed charges in a channel pore affect ionic fluxes through the open channel. Charge profiles can be tested by varying ion concentrations, which through shielding manifest as predictable changes in the shapes of the *I-V* relations and ion selectivities. The version of PNP we used only considers flux through a right cylindrical pore and cannot account for other or nonuniform pore geometries. In keeping the diffusion coefficients at their values for bulk solution, we examined the general effects that different pore charge distributions have on permeation.

Most remarkable was that a simple model that placed a single fixed negative charge density toward the extracellular end of the Cx46 hemichannel pore could account for its ion

selectivity and current rectification in symmetric KCl and in a variety of KCl gradients. It also could account for the properties of Cx46 cell-cell channels. Although smaller charges, both positive and negative, could be added and distributed to the model pore such that the PNP-generated *I-V* curves and channel selectivity properties agreed reasonably well with those obtained experimentally, all required a relatively large fixed charge located toward the extracellular end. The finding that both the rectification and selectivity of the Cx46*32E1 chimera could not be adequately described with a simple reversal in sign or removal of the charge in E1 indicates that there are, in fact, additional charges in the pore of the hemichannel that become influential in the absence of the dominant negative charge in E1. It is possible that the presence or absence of a large negative charge in E1 of other connexins may similarly play a key role in determining their selectivities. Cx32 may be an example of this, whereby the lack of the negative charge in E1 allows charged residues in NT to more strongly influence *I-V* relations and selectivity. Given the likelihood that all connexin pores will be constructed with the same sets of domains, it will be of interest to determine whether differences in the combination of charged residues in the NT and E1 domains underlie the differences in charge selectivities among native connexin channels.

REFERENCES

Adams, D. J., T. M. Dwyer, and B. Hille. 1980. The permeability of endplate channels to monovalent and divalent metal cations. *J. Gen. Physiol.* 75:493–510.

Andersen, O. S., and R. E. Koeppe, II. 1992. Molecular determinants of channel function. *Physiol Rev.* 72:S89–S158.

Beblo, D. A., and R. D. Veenstra. 1997. Monovalent cation permeation through the connexin40 gap junction channel: Cs, Rb, K, Na, Li, TEA, TMA, TBA, and effects of anions Br, Cl, F, acetate, aspartate, glutamate, and NO3. *J. Gen. Physiol.* 109:509–522.

Bennett, M. V., L. C. Barrio, T. A. Bargiello, D. C. Spray, E. Hertzberg, and J. C. Saez. 1991. Gap junctions: new tools, new answers, new questions. *Neuron.* 6:305–320.

Bennett, M. V., M. E. Spira, and D. C. Spray. 1978. Permeability of gap junctions between embryonic cells of *Fundulus*: a reevaluation. *Dev. Biol.* 65:114–125.

Bennett, M. V., X. Zheng, and M. L. Sogin. 1994. The connexins and their family tree. *Soc Gen Physiol Ser.* 49:223–233.

Bevans, C. G., M. Kordel, S. K. Rhee, and A. L. Harris. 1998. Isoform composition of connexin channels determines selectivity among second messengers and uncharged molecules. *J. Biol. Chem.* 273:2808–2816.

Beyer, E. C., and K. Willecke. 2000. Gap junction genes and their regulation. *In* Advances in Molecular and Cell Biology. E. L. Hertzberg, editor. JAI press, Stamford, CT. 1–30.

Bezrukov, S. M., and I. Vodyanoy. 1993. Probing alamethicin channels with water-soluble polymers: effect on conductance of channel states. *Biophys. J.* 64:16–25.

Boitano, S., E. R. Dirksen, and M. J. Sanderson. 1992. Intercellular propagation of calcium waves mediated by inositol trisphosphate. *Science.* 258:292–295.

Brink, P. R. 1983. Effect of deuterium oxide on junctional membrane channel permeability. *J Membr Biol.* 71:79–87.

Brink, P. R., and M. M. Dewey. 1980. Evidence for fixed charge in the nexus. *Nature.* 285:101–102.

Bruzzone, R., T. W. White, and D. L. Paul. 1996. Connections with connexins: the molecular basis of direct intercellular signaling. *Eur J Biochem.* 238:1–27.

Bukauskas, F. F., C. Elfgang, K. Willecke, and R. Weingart. 1995a. Biophysical properties of gap junction channels formed by mouse connexin40 in induced pairs of transfected human HeLa cells. *Biophys. J.* 68:2289–2298.

Bukauskas, F. F., C. Elfgang, K. Willecke, and R. Weingart. 1995b. Heterotypic gap junction channels (connexin26-connexin32) violate the paradigm of unitary conductance. *Pflug. Arch.* 429:870–872.

Cao, F., R. Eckert, C. Elfgang, J. M. Nitsche, S. A. Snyder, H. D. F., K. Willecke, and B. J. Nicholson. 1998. A quantitative analysis of connexin-specific permeability differences of gap junctions expressed in HeLa transfectants and Xenopus oocytes. *J Cell Sci.* 111:31–43.

Chen, D., J. Lear, and B. Eisenberg. 1997. Permeation through an open channel: Poisson-Nernst-Planck theory of a synthetic ionic channel. *Biophys. J.* 72:97–116.

Chen, D. P., L. Xu, A. Tripathy, G. Meissner, and B. Eisenberg. 1999. Selectivity and permeation in calcium release channel of cardiac muscle: alkali metal ions. *Biophys. J.* 76:1346–1366.

D' Andrea, P., and F. Vittur. 1996. Gap junctions mediate intercellular calcium signalling in cultured articular chondrocytes. *Cell Calcium.* 20:389–397.

Doyle, D. A., J. Morais Cabral, R. A. Pfuetzner, A. Kuo, J. M. Gulbis, S. L. Cohen, B. T. Chait, and R. MacKinnon. 1998. The structure of the potassium channel: molecular basis of K$^+$ conduction and selectivity [see comments]. *Science.* 280:69–77.

Ebihara, L., and E. Steiner. 1993. Properties of a nonjunctional current expressed from a rat connexin46 cDNA in *Xenopus* oocytes. *J. Gen. Physiol.* 102:59–74.

Eisenman, G., and R. Horn. 1983. Ionic selectivity revisited: the role of kinetic and equilibrium processes in ion permeation through channels. *J Membr. Biol.* 76:197–225.

Elfgang, C., R. Eckert, H. Lichtenberg-Frate, A. Butterweck, O. Traub, R. A. Klein, D. F. Hulser, and K. Willecke. 1995. Specific permeability and selective formation of gap junction channels in connexin-transfected HeLa cells. *J Cell Biol.* 129:805–817.

Finkbeiner, S. 1992. Calcium waves in astrocytes: filling in the gaps. *Neuron.* 8:1101–1108.

Flagg-Newton, J., I. Simpson, and W. R. Loewenstein. 1979. Permeability of the cell-to-cell membrane channels in mammalian cell junction. *Science.* 205:404–407.

Green, W. N., and O. S. Andersen. 1991. Surface charges and ion channel function. *Annu. Rev. Physiol.* 53:341–359.

Hu, X., and G. Dahl. 1999. Exchange of conductance and gating properties between gap junction hemichannels. *FEBS Lett.* 451:113–117.

Imoto, K., C. Busch, B. Sakmann, M. Mishina, T. Konno, J. Nakai, H. Bujo, Y. Mori, K. Fukuda, and S. Numa. 1988. Rings of negatively charged amino acids determine the acetylcholine receptor channel conductance. *Nature.* 335:645–648.

Kienker, P. K., W. F. DeGrado, and J. D. Lear. 1994. A helical-dipole model describes the single-channel current rectification of an uncharged peptide ion channel. *Proc. Natl. Acad. Sci. U.S.A.* 91:4859–4863.

Kienker, P. K., and J. D. Lear. 1995. Charge selectivity of the designed uncharged peptide ion channel Ac-(LSSLLSL)3-CONH2. *Biophys. J.* 68:1347–1358.

Kohen, E., C. Kohen, B. Thorell, D. H. Mintz, and A. Rabinovitch. 1979. Intercellular communication in pancreatic islet monolayer cultures: a microfluorometric study. *Science.* 204:862–865.

Lawrence, T. S., W. H. Beers, and N. B. Gilula. 1978. Transmission of hormonal stimulation by cell-to-cell communication. *Nature.* 272: 501–506.

Lo, C. W. 1999. Genes, gene knockouts, and mutations in the analysis of gap junctions. *Dev. Genet.* 24:1–4.

Mills, S. L., and S. C. Massey. 1995. Differential properties of two gap junctional pathways made by AII amacrine cells [see comments]. *Nature.* 377:734–737.

Nelles, E., C. Butzler, D. Jung, A. Temme, H. D. Gabriel, U. Dahl, O. Traub, F. Stumpel, K. Jungermann, J. Zielasek, K. V. Toyka, R. Dermietzel, and K. Willecke. 1996. Defective propagation of signals generated by sympathetic nerve stimulation in the liver of connexin32-deficient mice. *Proc. Natl. Acad. Sci. U.S.A.* 93:9565–9570.

Neyton, J., and A. Trautmann. 1985. Single-channel currents of an intercellular junction. *Nature.* 317:331–335.

Niessen, H., H. Harz, P. Bedner, K. Kramer, and K. Willecke. 2000. Selective permeability of different connexin channels to the second messenger inositol 1,4,5-trisphosphate. *J Cell Sci.* 113:1365–1372.

Niessen, H., and K. Willecke. 2000. Strongly decreased gap junctional permeability to inositol 1,4,5-trisphosphate in connexin32 deficient hepatocytes. *FEBS Lett.* 466:112–114.

Nonner, W., D. P. Chen, and B. Eisenberg. 1998. Anomalous mole fraction effect, electrostatics, and binding in ionic channels. *Biophys. J.* 74:2327–2334.

Nonner, W., and B. Eisenberg. 1998. Ion permeation and glutamate residues linked by Poisson-Nernst-Planck theory in L-type calcium channels. *Biophys. J.* 75:1287–1305.

Oh, S., Y. Ri, M. V. Bennett, E. B. Trexler, V. K. Verselis, and T. A. Bargiello. 1997. Changes in permeability caused by connexin 32 mutations underlie X-linked Charcot-Marie-Tooth disease. *Neuron.* 19:927–938.

Oh, S., J. B. Rubin, M. V. Bennett, V. K. Verselis, and T. A. Bargiello. 1999. Molecular determinants of electrical rectification of single channel conductance in gap junctions formed by connexins 26 and 32. *J. Gen. Physiol.* 114:339–364.

Paul, D. L., L. Ebihara, L. J. Takemoto, K. I. Swenson, and D. A. Goodenough. 1991. Connexin46, a novel lens gap junction protein, induces voltage-gated currents in nonjunctional plasma membrane of *Xenopus* oocytes. *J. Cell Biol.* 115:1077–1089.

Pitts, J. D., and J. W. Simms. 1977. Permeability of junctions between animal cells: intercellular transfer of nucleotides but not of macromolecules. *Exp. Cell Res.* 104:153–163.

Roux, B., and M. Karplus. 1994. Molecular dynamics simulations of the gramicidin channel. *Annu. Rev. Biophys. Biomol. Struct.* 23:731–761.

Roux, B., and R. MacKinnon. 1999. The cavity and pore helices in the KcsA K$^+$ channel: electrostatic stabilization of monovalent cations [see comments]. *Science.* 285:100–102.

Rubin, J. B., V. K. Verselis, M. V. Bennett, and T. A. Bargiello. 1992a. Molecular analysis of voltage dependence of heterotypic gap junctions formed by connexins 26 and 32. *Biophys. J.* 62:183–193.

Rubin, J. B., V. K. Verselis, M. V. Bennett, and T. A. Bargiello. 1992b. A domain substitution procedure and its use to analyze voltage dependence of homotypic gap junctions formed by connexins 26 and 32. *Proc. Natl. Acad. Sci. U.S.A.* 89:3820–3824.

Saez, J. C., J. A. Connor, D. C. Spray, and M. V. Bennett. 1989. Hepatocyte gap junctions are permeable to the second messenger, inositol 1,4,5-trisphosphate, and to calcium ions. *Proc. Natl. Acad. Sci. U.S.A.* 86:2708–2712.

Schwarzmann, G., H. Wiegandt, B. Rose, A. Zimmerman, D. Ben Haim, and W. R. Loewenstein. 1981. Diameter of the cell-to-cell junctional membrane channels as probed with neutral molecules. *Science.* 213:551–553.

Sheridan, J. D., M. E. Finbow, and J. D. Pitts. 1979. Metabolic interactions between animal cells through permeable intercellular junctions. *Exp. Cell Res.* 123:111–117.

Sneyd, J., M. Wilkins, A. Strahonja, and M. J. Sanderson. 1998. Calcium waves and oscillations driven by an intercellular gradient of inositol (1,4,5)-trisphosphate. *Biophys. Chem.* 72:101–109.

Subak-Sharpe, J. H., R. R. Burk, and J. D. Pitts. 1969. Metabolic cooperation between biochemically marked cells in tissue culture. *J. Cell Sci.* 4:353–367.

Suchyna, T. M., J. M. Nitsche, M. Chilton, A. L. Harris, R. D. Veenstra, and B. J. Nicholson. 1999. Different ionic selectivities for connexins 26 and 32 produce rectifying gap junction channels. *Biophys. J.* 77:2968–2987.

Trexler, E. B., M. V. Bennett, T. A. Bargiello, and V. K. Verselis. 1996. Voltage gating and permeation in a gap junction hemichannel. *Proc. Natl. Acad. Sci. U.S.A.* 93:5836–5841.

Unger, V. M., N. M. Kumar, N. B. Gilula, and M. Yeager. 1999. Three-dimensional structure of a recombinant gap junction membrane channel. *Science.* 283:1176–1180.

Vaney, D. I., J. C. Nelson, and D. V. Pow. 1998. Neurotransmitter coupling through gap junctions in the retina. *J. Neurosci.* 18:10594–10602.

Veenstra, R. D., H. Z. Wang, E. C. Beyer, and P. R. Brink. 1994a. Selective dye and ionic permeability of gap junction channels formed by connexin45. *Circ. Res.* 75:483–490.

Veenstra, R. D., H. Z. Wang, E. C. Beyer, S. V. Ramanan, and P. R. Brink. 1994b. Connexin37 forms high conductance gap junction channels with subconductance state activity and selective dye and ionic permeabilities. *Biophys. Jl.* 66:1915–1928.

Verselis, V., and P. R. Brink. 1986. The gap junction channel: its aqueous nature as indicated by deuterium oxide effects. *Biophys. J.* 50:1003–1007.

Verselis, V. K., C. S. Ginter, and T. A. Bargiello. 1994. Opposite voltage gating polarities of two closely related connexins. *Nature.* 368:348–351.

Verselis, V. K., and R. Veenstra. 2000. Gap junction channels: permeability and voltage gating. *In* Advances in Molecular and Cell Biology, E.L. Hertzberg, editor. JAI press, Stamford, CT. 129–192.

Wang, H. Z., and R. D. Veenstra. 1997. Monovalent ion selectivity sequences of the rat connexin43 gap junction channel. *J. Gen. Physiol.* 109:491–507.

White, T. W., and D. L. Paul. 1999. Genetic diseases and gene knockouts reveal diverse connexin functions. *Annu. Rev. Physiol.* 61:283–310.

Willecke, K., S. Kirchhoff, A. Plum, A. Temme, E. Thonnissen, and T. Ott. 1999. Biological functions of connexin genes revealed by human genetic defects, dominant negative approaches and targeted deletions in the mouse. *Novartis Found. Symp.* 219:76–96.

Wilson, G. G., J. M. Pascual, N. Brooijmans, D. Murray, and A. Karlin. 2000. The intrinsic electrostatic potential and the intermediate ring of charge in the acetylcholine receptor channel [In Process Citation]. *J. Gen. Physiol.* 115:93–106.

Young, S. H., H. S. Ennes, and E. A. Mayer. 1996. Propagation of calcium waves between colonic smooth muscle cells in culture. *Cell Calcium.* 20:257–271.

Zhou, X. W., A. Pfahnl, R. Werner, A. Hudder, A. Llanes, A. Luebke, and G. Dahl. 1997. Identification of a pore lining segment in gap junction hemichannels. *Biophys. J.* 72:1946–1953.